Structure of high density fibrin networks probed with neutron scattering and rheology

Katie M. Weigandt,[a] Danilo C. Pozzo*[a] and Lionel Porcar[bc]

Received 31st March 2009, Accepted 16th July 2009
First published as an Advance Article on the web 17th September 2009
DOI: 10.1039/b906256d

The structural and mechanical properties of coarse fibrin networks formed in D_2O solutions are investigated over a wide range of concentrations (1–40 mg mL^{-1}). For the first time, this range includes concentrations that are relevant to those found in *in vivo* blood clots. Small angle neutron scattering (SANS) and ultra small angle neutron scattering (USANS) are used to seamlessly characterize the structure over length scales ranging from 1 nm to several micrometres. Using invariant and Guinier analyses the internal volume fraction of protein within the fiber and their bulk average radius are determined directly. The network properties of fibrin clots are also characterized using a model for fractal structures. The network scale features are shown to be highly dependent on the initial fibrinogen concentration while the average fiber radius is only weakly dependent on this parameter. These results demonstrate the usefulness of combining SANS and USANS as characterization tools for complex biopolymer systems such as fibrin. The linear viscoelastic modulus of fibrin gels is related to the concentration by a power law equation that is valid over the entire range. In contrast, the non-linear rheology of dense networks is altered from the monotonic strain hardening response that is found at lower concentrations. This demonstrates the need for thorough characterization of fibrin at concentrations relevant to those of thrombi formed *in vivo*.

Introduction

Biopolymer networks have unique mechanical properties, such as high elasticity and reversible strain hardening, which are distinct from those of most synthetic polymer networks. These properties are related to the unique structure of the network, the fibers and the proteins within the fibers.[1–3] Fibrin is a frequently studied model biopolymer system that is responsible for the formation of blood clots upon traumatic injury.[4] The importance of this protein is twofold. First, the formation of thrombus *in vivo* is of critical importance to prevent excessive blood loss upon injury. However, improper coagulation in the body causes medical problems by preventing normal blood flow. This leads to cases of heart attack and stroke.[5] Second, fibrin networks also show significant promise as a novel scaffolding material for growing functional tissues.[6] In this application, fibrin clots are unique because they are inherently biocompatible, biodegradable, and present the mechanical properties that are necessary to promote tissue formation. For these and many other important reasons, fibrin has been extensively studied since its discovery in the late 19th century.[4] However, despite its obvious importance, the structural features of fibrin gels have been difficult to characterize in samples that are maintained in their native hydrated state. Previous research focused primarily on microscopy techniques that were unable to characterize fibrin gels over a large range of protein concentration and over a broad range of length scales.[2,7,8] In this new study, small angle neutron scattering and rheology are used to characterize the bulk structural and mechanical properties of coarse fibrin clots formed from D_2O saline solutions over a broad range of fibrinogen concentrations (1–40 mg mL^{-1}). Using a combination of small angle neutron scattering (SANS) and ultra small angle neutron scattering (USANS) the bulk structural features of unperturbed fibrin are seamlessly characterized over a large range of length scales between 1 and 15 000 nm.

Like many other biopolymers, fibrin is often regarded as a semiflexible polymer because its persistence length can be of the same order of magnitude as the contour length, or in this case the distance between the network junctions.[3] This semi-flexibility is believed to be the origin of some of the unique rheological properties of fibrin.[9] It is essential to have an extensive rheological characterization of these biopolymers to fully understand the physiological behavior of these materials. Many biopolymers such as actin, collagen, and fibrin show unique linear and non-linear rheological properties.[9] For example, under low levels of deformation or strain, the elasticity of fibrin clots is characterized by a constant elastic modulus. However, upon application of larger levels of strain, these biopolymers stiffen and undergo a phenomenon known as strain hardening.[9,10] This behavior is fully reversible up to moderate strains (~50% strain for fibrin).

Several models and theories have been developed in an effort to understand the cause of this unique mechanical behavior.[9,10] At very low strains, the shear modulus of the gel is usually related to the initial concentration of proteins with a power law relationship.[3] The power law exponent is related to the nature of the interaction between the fibers. For a network of crosslinked

[a]*Chemical Engineering Department, University of Washington, Seattle, WA, 98195, USA. E-mail: dpozzo@u.washington.edu*
[b]*Institut Laue-Langevin, Grenoble, France*
[c]*National Institute of Standards and Technology, Gaithersburg, Maryland, USA*

fibers, the elastic modulus is predicted to have a stronger dependence ($G \approx C^{2.5}$) on the protein concentration compared to the case where the fibers are physically entangled ($G \approx C^{2.2}$). The structural origin of the non-linear strain hardening response in biopolymer gels is currently under debate and several alternative theories have been postulated.[9,10] We believe that SANS and USANS, in combination with rheology, provide valuable information to further develop these theories and relate the structural and mechanical properties of fibrin and other biopolymer networks.

Fig. 1 shows a schematic of the three-dimensional structure of a coarse fibrin network over all relevant length scales. Fibrinogen, which is found naturally in the blood stream, is converted to fibrin by the enzyme thrombin. This enzyme is released locally near the region of trauma as the last factor in the coagulation cascade.[4] Fibrin then self-assembles into a half-staggered linear array of proteins called a protofibril. Several protofibrils may also aggregate radially and form what are referred to as coarse fibers.[11,12] The total extent of lateral aggregation is controlled by the solvent properties including the ionic strength, pH and the isotopic composition of water.[2,12,13] It is also known that the resulting fibrin fibers have a low internal protein volume fraction (Φ_{Int}). Most estimates suggest that 70–80% of the total fiber volume is water.[4,14,15] Unfortunately, there are large fluctuations in the reported values and no examination of systematic variations has been undertaken. The internal protein fraction has been estimated by evaluating the turbidity of fibrin samples[14] and also by optically matching the index of refraction of clots containing very low fibrin concentrations.[15] In this paper, we describe a new method based on neutron scattering to directly and accurately obtain this information from fibrin clots that are formed over a much wider range of protein concentrations. This method determines the internal porosity of the fibers from the angular dependence of the scattering intensity $I(q)$.

Previous works have reported on the structural and mechanical characterization of fibrin at relatively low concentrations (<10 mg mL^{-1}).[2,16] The normal range of fibrinogen concentration in the blood stream usually varies between 2 and 4 mg mL^{-1}. Electron microscopy was commonly used to determine the basic structural properties of fibrin gels. This technique demonstrated that upon the addition of thrombin, fibrin forms a bifurcating network of cylindrical fibers with no visible dangling ends.[2] Unfortunately, the properties of the hydrated gel cannot be easily evaluated with electron microscopy. Optical techniques such as confocal microscopy, which do not require sample processing, have also been utilized to this end.[7] However, these techniques are limited by the minimum length scale of the fibrinogen features that can be characterized and by the opacity of gels at high concentrations of protein. It has been shown that the concentration of fibrin in a thrombus that is formed *in vivo* is much higher (20–70 mg mL^{-1}) than any concentration that has been characterized in previous work.[17] This is also much higher than the normal concentration of fibrinogen in the blood (2–4 mg mL^{-1}).

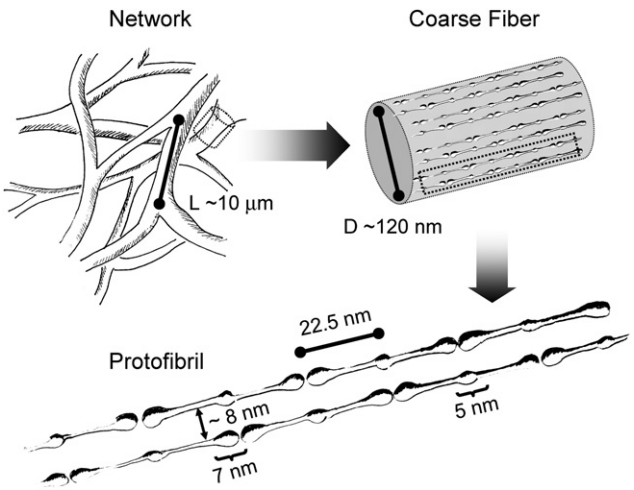

Fig. 1 Schematic of fibrin network features at different scales ranging from 1 nm to 10 μm.

Small angle scattering techniques are ideally suited to characterize the bulk structural properties of clots formed at high concentration and in their native hydrated state. Furthermore, the use of deuterated solvents promotes the lateral growth of fibers within the clots. The use of D_2O buffers improves the resolution of the structural characterization due to the significant difference in the scattering length density between the hydrogen in the protein and the deuterium in the solvent.[13] The complex structural features of fibrin clots also motivate the need for a rigorous approach to seamlessly probe the hydrated structure of fibrin clots over a wide range of length scales and concentrations. Neutron scattering is ideally suited for this because of the wide range of length scales that can be characterized with the same technique. In this study, the SANS technique provides information about the internal structure and the radial dimension of the fibers, while the USANS technique is used to characterize larger features including the fractal dimension of the network (D_f) and the correlation length (ξ) over which the fractal structure persists. Both techniques are performed on the exact same samples.

Materials and methods

Sample preparation

Human α thrombin and fibrinogen solutions depleted of plasminogen and von Willebrand factor were purchased from Enzyme Research Laboratories (South Bend, IN). Deuterated water containing 99.9% D_2O was obtained from Cambridge Isotope Laboratories (Andover, MA). The fibrinogen was dialyzed against a deuterated buffer composed of 0.5 M NaCl, 0.05 M Tris, and 99.9% D_2O with a pD of 7.4 in regenerated cellulose dialysis tubing over 12 h. The composition of the buffer was selected to maximize the stability of the proteins while also promoting the formation of coarse fibers containing several protofibrils.[13] Dialysis was performed until the final stock solution contained at least 98% deuterated water. The fibrinogen stock solutions in D_2O buffer were separated into aliquots and stored at −80 °C. Prior to final sample preparation, the protein solutions were thawed, diluted and filtered through a 0.45 μm syringe filter to remove any protein aggregates or dust. The final fibrinogen concentration was then determined from the absorbance at 280 nm using a UV/VIS spectrophotometer and an extinction coefficient of 1.6 mL mg^{-1} cm^{-1}.[14] Trace amounts of the protein Factor XIII are known to be present in the initial

fibrinogen solution. This protein, when activated with calcium, promotes the formation of ε-(γ-glutamyl)lysine isopeptide bonds between adjoining protein monomers in fibrin fibers.[18] To ensure the activation of the factor XIII protein, $CaCl_2$ is added to the filtered protein solution to a final concentration of 2.5 mM Ca^{2+}. Prior to polymerization, the fibrinogen solutions are degassed under a −30 mmHg vacuum for 40 min. Degassing the sample is necessary to prevent the nucleation of microbubbles that can overcome the fibrin signal and render the USANS data analysis unworkable. To initiate coagulation, 0.16 NIH units of thrombin per millilitre of the total solution were added to each fibrinogen sample just prior to loading it into the SANS cells or the rheometer. The thrombin concentration is sufficiently low to allow proper loading of samples into the rheometer and the neutron scattering cells before the polymerization begins to occur. After initiation, the gel was allowed to form in the sample holders over a period of 10 h prior to testing.

Rheology

Rheological data were obtained with an Anton Paar MCR 301 stress controlled rheometer using a cone and plate geometry with a 2.5 cm diameter and a 1° angle. During polymerization, the samples were subjected to 0.1% strain oscillations at a frequency of 1 Hz for 10 h in order to track the development of the clot and to ensure that the gel formation had reached completion. This was determined by reaching a plateau in both the elastic (G') and the viscous (G'') moduli. A strain of 0.1% was appropriate to track the gelation process while also being sufficiently small to prevent the alteration of the rheology and structure of the final gel. After complete polymerization, the linear moduli of the gel (G' and G'') were measured with a frequency sweep (0.0001 and 100 Hz) at a fixed strain of 1%. Subsequently, the instantaneous (non-linear) modulus of the gel was probed by performing a steady stress ramp and holding steady for 1 min intervals at each stress level. The strain was measured just prior to each step in applied stress. In order to verify that the measured mechanical properties were not related to interfacial slip, the rheology was measured using various instrument configurations and surface materials. Additionally, step stress tests were also tracked as a function of time to ensure that the samples did not experience any creep, slip or yielding during the application of the stress. None of these effects was found to occur in these samples.

Neutron scattering

Small angle neutron scattering (SANS) and ultra small angle neutron scattering (USANS) measurements were performed on the same samples at the Center for Neutron Research at NIST in Gaithersburg, Maryland. SANS measurements were performed on the NG3 30 meter instrument.[19] Measurements were made at three detector distances of 1.3, 7 and 13.2 m to cover a broad q range (0.002–0.3 $Å^{-1}$) using neutron wavelengths of 5 Å and 8.4 Å. All of the SANS data were corrected for background and sample cell scattering, and placed on an absolute scale relative to the direct beam flux.[20] USANS measurements were performed on the BT5 perfect crystal diffractometer extending the measured q range down to 4×10^{-5} $Å^{-1}$.[21] Data are reduced and desmeared using the NIST Igor based software.[20]

Results

Rheology

Fibrin gels were mechanically characterized to determine the variations in the moduli as a function of fibrinogen concentration. At low strain, fibrin gels exhibit linear viscoelasticity and the modulus of the gel is independent of strain. The storage modulus of the gel was characterized within the linear viscoelastic limit at 1% strain over a frequency range bounded by 0.0001 and 100 Hz. Fig. 2 shows the normalized storage and loss modulus as a function of frequency as well as the storage modulus at 1 Hz as a function of fibrinogen concentration. The modulus increases slightly with increasing frequency but it is relatively constant overall. The collapse of the normalized data shows that the frequency dependence is the same at high and low concentrations. Also, the storage modulus is consistently greater than the loss modulus indicating that the material is a gel over the entire frequency range. The modulus dependence on fibrinogen concentration is well fit by a power law equation with $G' \approx c^{2.22}$. This is almost identical to the expected dependence for solutions of entangled semiflexible fibers ($G' \approx c^{2.20}$) but it is lower than the prediction for crosslinked networks ($G' \approx c^{2.5}$).[3]

It is well known that fibrin gels exhibit non-linear behavior with increasing strain. More specifically fibrin gels are reversibly strain hardening. A slow step stress ramp was used to characterize the non-linear rheology of fibrin as a function of strain. Fig. 3 shows the instantaneous modulus ($G_{Inst} = d\gamma/d\sigma$) as a function of strain. It is evident that the non-linear rheology of the fibrin gel is highly dependent on the initial fibrinogen concentration. At a concentration of 3 mg mL^{-1}, the fibrin gel begins to harden at about 3% strain and the gel modulus

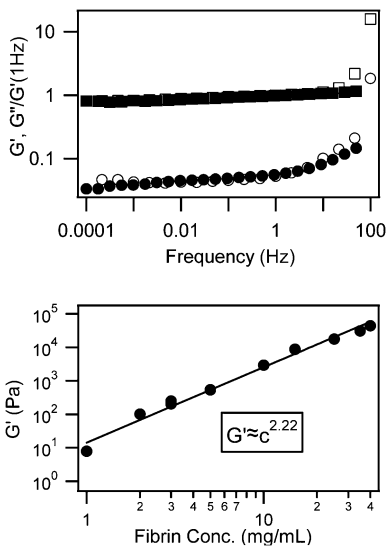

Fig. 2 Rheology of fibrin clots within the linear viscoelastic limit. A: the frequency dependence of modulus of 2 [G' (□), G''(○)] and 25 [G' (■), G'' (●)] mg mL^{-1} fibrin clots normalized by G' at 1 Hz. B: storage modulus (G') of ligated fibrin clots formed from fibrinogen of varying concentration (1–40 mg mL^{-1}) and fit with a power law equation.

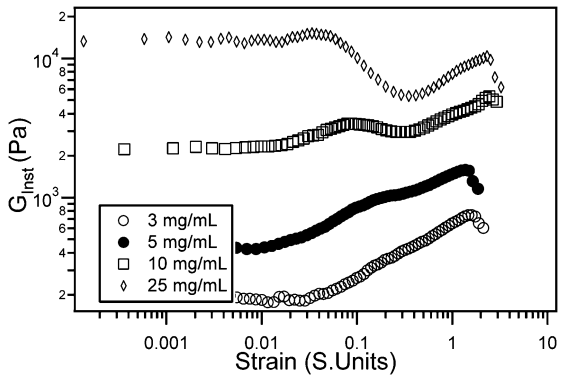

Fig. 3 Instantaneous modulus (G_{Inst}) plotted *versus* strain for four fibrin samples of increasing concentration.

increases gradually. The gel begins to break at high deformation giving rise to a steep decrease above 150% strain. The 5 mg mL^{-1} fibrin gel behaves similarly, but the rate of the modulus increase becomes weaker between 10 and 40% strain. At 10 mg mL^{-1}, a new region of strain softening appears between 10 and 30% strain before the samples begin to stiffen again. In fibrin gels with very high concentrations of fibrinogen (≥25 mg mL^{-1}), the modulus of the gel does not increase at 3% strain as previously observed. Instead, these samples show a steep reduction in the modulus at about 6% strain before the modulus begins to increase again at 30% strain. In this later range, the behavior matches the high strain behavior of the lower concentration samples. To the best of our knowledge, this complex rheological behavior at high fibrin concentrations has not been reported previously. It must also be noted that the concentration of fibrin in clots that are formed *in vivo* falls in the range where this rheological transition is observed.

Neutron scattering

The scattering data (SANS and USANS) for each sample were fully reduced, corrected for instrumental resolution (desmeared) and combined into a single scattering profile. The data covered an extremely broad range of q values between 0.00004 and 0.3 Å^{-1} that can be associated with features of sizes ranging roughly between 1 and 15 000 nm. Fig. 4 shows the combined USANS and SANS scattering profiles for 3, 10 and 30 mg mL^{-1} fibrin gels normalized to the concentration of the samples. For most samples, the main differences in the scattering occur at the lowest q values obtained from USANS. The data shown in Fig. 4 are representative of profiles collected for fibrin samples in the range of 1 to 40 mg mL^{-1}.

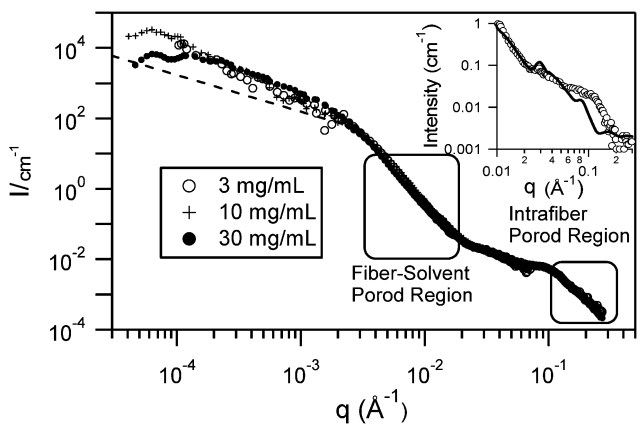

Fig. 4 Combined SANS and desmeared USANS scattering profiles for fibrin gels formed from different concentrations of fibrinogen (3 mg mL^{-1}, 10 mg mL^{-1}, and 30 mg mL^{-1}) with intensity (cm^{-1}) normalized by concentration (mg mL^{-1}). The dashed line is a −1 power law. Inset: model for the tetragonal protofibril lattice compared to the high q data for 8 mg mL^{-1} fibrin.[12]

The features in the profiles of Fig. 4 can be associated with the structural regions of the fibrin network that are highlighted in Fig. 1. At high q (>0.01 Å^{-1}) there are two distinct plateaus in the intensity profile that correspond to the internal structure of the individual fibers. At intermediate values (0.001 < q < 0.01 Å^{-1}) the SANS data are mostly characterizing the structure of individual fibers. The slope transition that occurs at 0.002 Å^{-1} is related to the average radius of the cylindrical fibers. Finally, at very low q, in the USANS regime, the scattering is dominated by the structure of the network. In this region, the data can be used to determine the fractal dimension of the network. Additionally, at low q a plateau is observed for samples with high protein concentrations (c > 10 mg mL^{-1}). This is characteristic of an inhomogenous distribution of protein over large scales, and it corresponds to the correlation length of the fractal structure. At lower fibrin concentrations, the low q plateau occurs at length scales that are larger than the resolution limit of the USANS instrument.

Fig. 4 shows the most significant changes in the very low q range (USANS) corresponding to the network structure. All other features of the scattering profile remain relatively unchanged with increasing fibrinogen concentration. The 3 mg mL^{-1} fibrin curve does not have a low q plateau in the measurable q range. The curves of both the 10 and the 30 mg mL^{-1} samples present a plateau that shifts to higher q values as the concentration increases. In addition to the low q variation, there are also slight variations in the scattering curves in the higher q regions that are difficult to appreciate in the log–log representation. While visual inspection of the curves permits a qualitative assessment of possible structural differences, careful quantitative analyses of the scattering data can provide detailed structural information. We perform a substantial analysis of the data using general model-independent analyses based on simple scattering laws. This allows direct extraction of valuable information without having to make *a priori* assumptions of structural models that could lead to uncertainty in the results. Using a simple Guinier and Porod analysis, an effective cylinder radius and the internal protein volume fraction of the fibers can be determined directly.

Internal fiber structure

The inset of Fig. 4 highlights the scattering data at high q. In this range, the structural information is dominated by the relative position of fibrinogen proteins and protofibrils within individual fibers. One evident feature in this q range is the appearance of a broad correlation peak at $q = 0.028$ Å^{-1} that corresponds to the repeat spacing (~22.5 nm) of the well known half-staggered fibrin structure.[4] This peak is even more pronounced in neutron

diffraction experiments of magnetically aligned fibers and on SAXS carried out on dry fibrin films.[22,23] For coarse clots, with significant lateral aggregation, the SANS and SAXS profiles are sensitive to the packing of the individual protofibrils. A tetragonal lattice (unit cell 18.4 × 18.4 × 44.6 nm) was proposed by Yang *et al.* based on crystallographic data of the proteins. This lattice is also backed experimentally by peaks observed earlier in neutron diffraction experiments and more recently by energy dispersive X-ray diffraction (EDXD).[12,22,24]

In order to compare the proposed structure to our data, the scattering intensity of the protofibril lattice was modeled and compared to the high q region of our experimental curves. The scattering intensity for this ordered lattice can be approximated using the Debye equation for a lattice of spheres.[25] For this purpose, the structure of fibrinogen is simplified by assuming that the molecule is composed of two types of spherical domains with different sizes but identical scattering length density (SLD). These two types of spheres correspond to the central (R_c = 2.5 nm) and terminal (R_t = 3.5 nm) domains of the fibrinogen protein. For simplicity, the scattering from the coiled coils that link these domains is omitted from the model as its contribution is expected to be relatively small. The simulated scattering (Fig. 4 inset) agrees qualitatively well with the measured intensity but has notable differences at very large angles ($q > 0.1$ Å^{-1}). This demonstrates that SANS experiments could help to refine the internal structure of the fibers.

For all samples, the scattering profiles also contain two easily distinguishable Porod regions. The low q Porod region is a result of the interface between the coarse fibers and the solvent that fills the pores of the network. The high q Porod region is caused by the sharp interface that exists between the individual proteins and the solvent that fills the gaps within each fiber. Similar double Porod regions occur in the scattering of porous and granular media. For systems exhibiting clearly distinguishable features on two distinct length scales, a method of analysis has been developed to determine the volume fraction of small pores within the "grain" (larger structures) as well as the volume fraction of the "grains".[26] We have extended this established method to determine the protein volume fraction (Φ_{Int}) inside fibrin fibers formed over a broad range of concentrations.

For an isotropic two-phase system, the scattering invariant (Q) relates the scattering intensity (I) to the total protein volume fraction (Φ_{Fib}) and the scattering contrast between the two phases ($\Delta\rho$).[17] The total invariant is calculated directly by integrating the scattering profile using eqn (1):

$$Q = \int_0^\infty I_m(q) q^2 \, dq = 2\pi^2 \Phi_{Fib}(1 - \Phi_{Fib})(\Delta\rho)^2 \quad (1)$$

This calculation requires extrapolation of the intensity at low and high q values. The scattering contrast is determined from the scattering length density (SLD) of the deuterated solvent and the fibrinogen proteins. The SLD of the solvent was calculated to be 6.3 × 10^{-6} Å^{-2} using the known atomic composition and the measured density. The SLD of fibrinogen in D_2O buffer at pD 7.4 was measured experimentally as 3.17 × 10^{-6} Å^{-2} by dispersing fibrinogen in solutions containing different amounts of D_2O. The total volume fraction of fibrinogen in the gel (Φ_{Fib}) is calculated from the total invariant Q and eqn (1). This parameter is known from the sample preparation. Therefore, this process represents a good consistency check for the accuracy of the integration and the value of the scattering contrast ($\Delta\rho$). The calculated value of Φ_{Fib} was found to be on average within 10% of the value from the sample preparation.

To measure the volume fraction of proteins within individual fibers (Φ_{Int}), the intensity corresponding to the sharp interface between the proteins and the solvent within fibers needs to be isolated. This requires the separation of the scattering contributions corresponding to the larger structural features. This is possible because the two Porod regions are well separated in length scale. The modified intensity profile (I^*) is dominated by the contributions of the internal fiber structure.

$$I^*(q) = I(q) - I(q_*)\frac{q_*^4}{q^4} \quad (2)$$

In eqn (2), I is the absolute scattering intensity and $I(q_*)$ is the measured intensity at q_* where q_* is any value in the low q Porod region. The above separation is analogous to performing the following imaginary sample modification. A scattering profile similar to that of the modified intensity (I^*) would be obtained if it were possible to remove all buffer that lies between the fibers in the network without affecting the structure of the individual fibers. This would leave a compressed layer of protein and water with a porous nanostructure identical to that of the internal structure of the fibers. The invariant of the modified intensity (I^*) can then be used to determine the volume fraction of protein within the fibers (Φ_{Int}). The internal protein volume fraction (Φ_{Int}) is evaluated from the measurement of the invariant of the high q Porod region (Q^*) with eqn (3):

$$Q^* = \int_0^\infty I^* q^2 \, dq = 2\pi^2 \Phi_{Fib}(1 - \Phi_{Int})(\Delta\rho)^2 \quad (3)$$

The internal protein fraction (Φ_{Int}), calculated from this invariant analysis, is plotted as a function of fibrinogen concentration in Fig. 5. The internal protein fraction in the fibers increased steadily with concentration and the relationship was fit

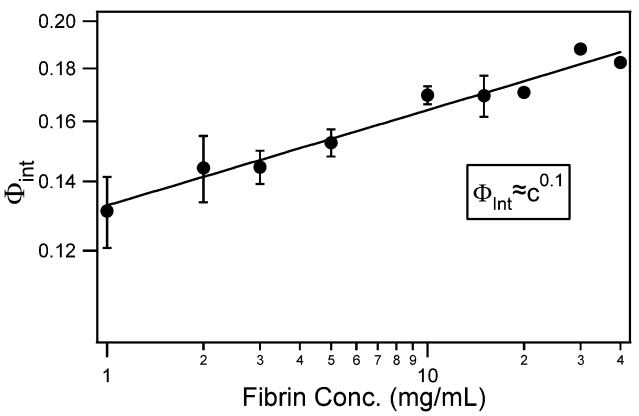

Fig. 5 Internal volume fraction of fibrin fibers from multilevel invariant analysis. The error bars are determined from the uncertainty of the invariant extrapolation.

with a power law. Interestingly, the values are lower than the previous estimates of ~20% protein.[4,14]

Fiber structure

A Guinier fit on the fiber cross-section was performed at the turnover between the low q region and the first Porod region to determine the average radius of the fibrin fibers. For elongated structures, the intensity and q in the Guinier region are related to the cross-sectional radius of gyration by eqn (4):[27]

$$(qI)_{Q\to 0} = (qI)_0 \exp\left(- \left(\frac{R_g^2}{2}\right) q^2 \right) \quad (4)$$

In this equation, q is the scattering angle, I is the intensity, and R_g is the cross-sectional radius of gyration. This method is analogous to the common Guinier analysis that is used for globular particles. However, the data here are plotted in the form of $\ln(qI)$ *vs.* q^2 and it is only applicable to highly elongated particles. The great benefit of using this simple method instead of a model fitting approach is that the average radius is obtained directly without having to account for polydispersity or having to assume a size distribution. Fits to monodisperse cylinder models were determined to be inadequate. The Guinier approach significantly reduces the uncertainty of the results because it minimizes the number of parameters. For cylindrical objects, the average radius of gyration is related to the average radius of the fibers by eqn (5).[27]

$$R = R_g\sqrt{2} \quad (5)$$

In this equation, R is the radius of the fiber and R_g is the cross-sectional radius of gyration calculated from eqn (4). The average radius is plotted *versus* the initial fibrinogen concentration in Fig. 6. From the figure, it is apparent that the radius varies very little with concentration. However, careful inspection shows that there is a slight decrease in the radius with increasing fibrinogen concentration between 2 and 20 mg mL^{-1}. In contrast, at higher concentrations (30 and 40 mg mL^{-1}) the radius of the fibers was significantly larger.

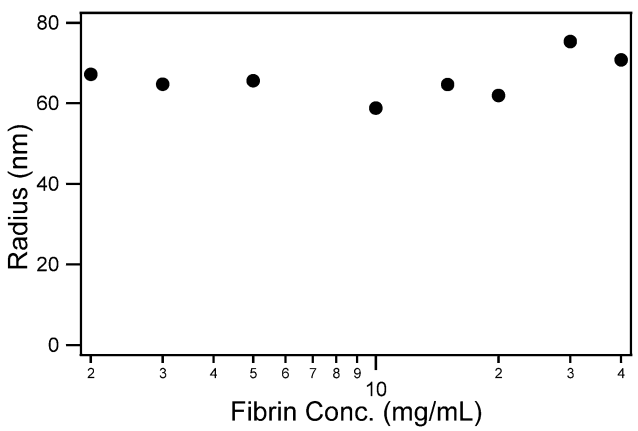

Fig. 6 Radius of fibrin fibers determined from a Guinier analysis on the fiber cross-section. The error bars as determined from the Guinier fit are masked by the data markers.

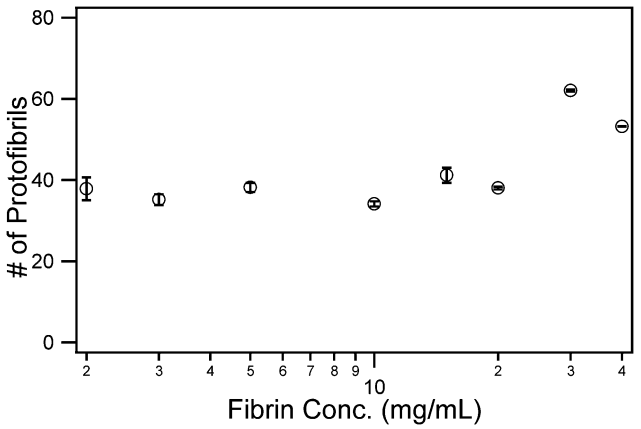

Fig. 7 Average number of protofibrils in a radial slice of fibrin fiber calculated from the mass to length ratio of the fibers and protofibrils.

From the values of Φ_{Int} and R, it is also possible to calculate the average number of protofibrils (N_P) in the radial cross-section of a coarse fibrin fiber. This is calculated using eqn (6):

$$N_P = \frac{\mu_{Fiber}}{\mu_P} = \frac{\Phi_{Int}\rho_m R^2}{\mu_P} \quad (6)$$

In this equation N_P is the average number of protofibrils in a radial cross-section of the fiber, ρ_m is the mass density of individual fibrinogen proteins (1.4 g mL^{-1}), R is the average fiber radius obtained from the Guinier analysis, and μ_P is the mass–length ratio of a single protofibril.[28] The mass to length ratio of a single protofibril is assumed to be constant and is calculated by considering the half-staggered structure of fibrin and the known repeat distance of 22.5 nm (μ_P = 340 kDa/22.5 nm). We find that the average number of protofibrils changes negligibly for gels formed from initial fibrinogen concentrations of 20 mg mL^{-1} or less, Fig. 7.

Network structure

In the USANS region, the scattering characterizes the structure of the network. The slope of the intensity deviates significantly from −1, indicating that the data cannot be modeled as discrete rigid cylinders. This deviation could be caused by significant fiber flexibility (form factor) or by having a branched network structure (structure factor). In coarse clots, the fibers are rigid and flexibility alone could not account for this change because the persistence length would be unreasonably low. Therefore, changes in the low q range are related primarily to changes in the network structure.

A fractal model based on the work of Teixeira was used to evaluate the network scale structure of the fibrin gel. This is primarily reflected in the data collected with the USANS instrument ($q < 3 \times 10^{-3}$ Å^{-2}).[29] A least squares fitting algorithm is used to fit the data with the fractal model described by eqn (7)–(9). The total scattering intensity is given by the product of the form factor $P(q)$ and the fractal structure factor $S(q)$.

$$I(q) = P(q)\ S(q) \quad (7)$$

The form factor of spherical subunits is used to construct the fractal network.

$$P(q) = \phi V_P^2 \Delta\rho^2 \left(\frac{\sin(qR_0) - qR_0\cos(qR_0)}{3(qR_0)^3} \right)^2 \quad (8)$$

In eqn (8), ϕ is the volume fraction of the primary spheres, V_P is the volume of the individual spherical particles, $\Delta\rho$ is the contrast between the two phases (fibers and solvent), q is the wave vector and R_0 is the radius of the individual spheres. $S(q)$ is the structure factor of the fractal which is defined in eqn (9).

$$S(q) = 1 + \frac{\sin\left[(D_f - 1)\tan^{-1}(q\xi)\right]}{(qR_0)^{D_f}} \frac{D_f\Gamma(D_f - 1)}{\left[1 + 1/(q^2\xi^2)\right]^{(D_f-1)/2}} \quad (9)$$

In this equation, D_f is the fractal dimension and ξ is the correlation length over which the fractal structure persists. The incoherent background was subtracted from the data prior to analysis and was fixed at zero for all models. The scattering length densities for the protein and solvent were the same as used in the invariant analysis. The radius of the spheres, R_0, was set equal to the radius of the cylinders calculated from the Guinier analysis from eqn (4) and (5). Thus only ξ, D_f, and ϕ were varied until χ^2 was minimized. While this analysis does not specifically apply to a distribution of cylindrical fibers, it is possible to consider that the fibers themselves are composed of chains of spherical particles. This is a valid assumption at the low q values (USANS regime) used for model fitting because in this region the scattering is not sensitive to the shape of the individual building blocks.

Fig. 8 shows that the fractal dimension (D_f) increased slowly for gel concentrations up to 15 mg mL^{-1} protein. In this range, the fractal dimension had values that were very close to 2. These are similar to the values found for fibrin clots formed in H_2O at low concentrations.[30] At high concentrations the fractal dimension increases steeply according to a power law. At 40 mg mL^{-1} the fractal dimension approaches a value of 2.8 which indicates that there are densely packed fibers in the gel. The density of branch points in fibrin gels is affected by the protein concentration and the polymerization kinetics. The lack of a strong variation in the internal fiber composition indicates that the distribution of fibers must change at the network level. Therefore, the density of fibers must increase and the distance between branch points decreases with increasing concentration. This results in the observed increase of the fractal dimension.

The correlation length (ξ), which describes the finite domain over which the fractal dimension is valid, decreased consistently with increasing concentration. However, this parameter was only statistically significant at high protein concentrations ($c > 10$ mg mL^{-1}). At the highest concentrations, the correlation length of the fractal structure approaches the diameter of the fibers. The relationship between fibrinogen concentration and fractal correlation length is also well approximated by a power law. This function was extrapolated to estimate the correlation length of fibrin gels at lower concentrations. Assuming that this power law persists, the correlation length of a 1 mg mL^{-1} fibrin gel is estimated to be about 49 μm. At these low concentrations fibrin gels can be imaged optically. Fig. 9 shows a digital image of a 1 mg mL^{-1} fibrin gel taken from an inverted optical microscope using a 40× objective. It is clear that the protein is distributed inhomogenously throughout the gel, with regions of high fiber density separated by less dense regions. The separation between the discrete pockets of high concentration is roughly of the same order of magnitude as the extrapolated correlation length. This suggests that the correlation length that is determined from the fractal model is representative of heterogeneity in the gel and it is not equal to the mesh size of the network. Therefore, it cannot be related to the linear modulus in the rheological model described by Mackintosh *et al.*[3]

Both the increasing fractal dimension and the decreasing correlation length indicate that, as the fibrin concentration increases, the network becomes denser and has closely spaced high density pockets. In gels formed from the highest concentration protein solutions, the fractal correlation length is approaching the same order of magnitude as the fiber diameter. This suggests that the polymerization kinetics and aggregate mobility may be significantly altered in higher concentration solutions during formation of the gel. The monomer to initiator ratio increased with fibrinogen concentration because the thrombin concentration was held constant. The kinetic changes associated with the increased protein concentration are likely

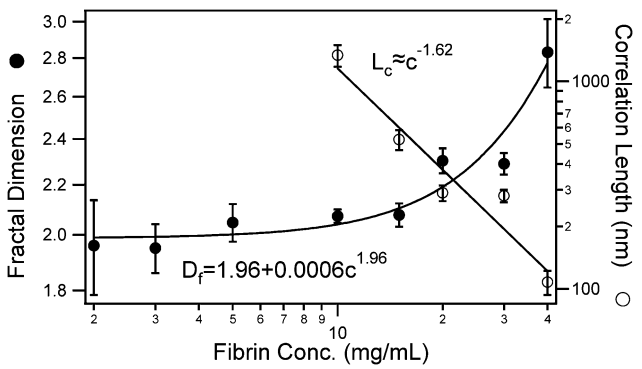

Fig. 8 Fractal dimension (D_f) [●] and correlation length (l_c) [○] of fibrin fibers determined by fitting the USANS scattering profile with the Teixeira fractal model.[29]

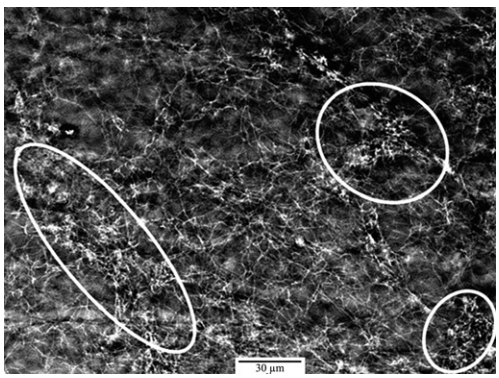

Fig. 9 Optical microscopy image of a 1 mg mL^{-1} fibrin gel. Circled regions indicate higher density pockets of fibrin.

responsible for many of the differences in the network structure. This is also likely a reason for the significant change in the structure of the individual fibers at concentrations above 20 mg mL^{-1}. At this point there is little space in the gel for new fibers to form. Therefore, it may become more favorable for existing fibers to grow into larger structures than for new smaller fibers to form.

Discussion

Rheology

In the past, rheological measurements have shown that fibrin gels are reversibly strain hardening like many other biopolymer networks. Most of these studies have found that, when the fibrin gel is strained, the storage modulus starts to increase sharply in the region between 1 and 10% strain.[9,16] These studies have motivated a significant amount of work aimed at deciphering the origin of this unique mechanical response. However, most previous work has focused on the rheological properties of fibrin clots formed from initial fibrinogen concentrations of less than 5 mg mL^{-1}. In this study, the structure and rheology are characterized for fibrin formed over a wide range of fibrinogen concentrations. From Fig. 3, it is clear that the non-linear rheological response with increasing strain is highly dependent on the fibrin concentration. For fibrin formed at low concentrations, the instantaneous modulus of the fiber increased steadily with increasing strain. This is consistent with the results of previous work.[9,16,31] In contrast, significant differences were observed for fibrin gels formed from higher concentrations of fibrinogen. When these gels were strained to about ~10% the gel began to soften. This response continued until it was strained to about ~30% where it began to harden again.

This result must be considered within the context of the two theories that have been proposed to describe the strain hardening of fibrin gels. The theory proposed by Storm *et al.* postulates that the reversible strain hardening behavior of semiflexible biopolymer networks is caused by an entropic response that is related directly to the persistence length of the fibers.[9] These fibers will become fully extended when enough force is applied to remove them from their thermodynamically stable flexible state. The response of all the individual fibers then results in the macroscopic non-linear rheology of the network. Onck *et al.* propose an alternative theory where the thermodynamic undulations of the fiber are not the primary cause of strain hardening. Instead, these authors suggest that the reorientation of fibers and subsequent bending and stretching of fiber segments are the primary cause of the non-linear rheological response.[10] It should be pointed out that these two theories are not mutually exclusive and that it is possible that both factors contribute in some extent to the strain hardening response. Still, neither model predicts the strain softening that is observed at higher concentrations in this study.

Theories have also been developed to correlate the linear rheological properties of semiflexible polymer networks to the structural features of these materials.[3,9] For a network of semiflexible fibers, such as fibrin, it is expected that the elastic modulus of the gel will increase with monomer concentration by a power of $c^{2.5}$. We used rheological measurements to compare the coarse fibrin clots with this prediction. Previous studies reported a power law dependence with the exponent ranging between 1.66 and 2.1 for fibrin clots formed in H_2O buffers.[2,32] The power law relationship for coarse fibrin clots formed in D_2O had an exponent of about 2.22 in the range of fibrinogen concentrations between 1 and 40 mg mL^{-1} (Fig. 2). This falls between the theoretical prediction and the measured values found previously for fine clots.[3] It is also important to note that this power law dependence is found to be valid throughout the expanded concentration range.

Structure characterization

The structural properties of the individual fibers are found to change with concentration. In previous studies the fiber radius and internal composition were measured primarily with optical and scanning electron microscopy.[2,15] Unfortunately, both of these techniques have limitations that make it difficult to characterize high concentration samples in their natural hydrated state. In addition, previous studies have only focused on characterizing fibrin gels formed from solutions containing fibrinogen at concentrations typically observed in human plasma, 2–4 mg mL^{-1}. This work expands upon the previous research by increasing the studied range to fibrinogen concentrations of 40 mg mL^{-1}. The expanded concentration range is now physiologically relevant as it has been reported that fully formed thrombi contain between 20 and 70 mg mL^{-1} fibrin.[17] Neutron scattering was successfully used to characterize the bulk structural properties of fibrin gels over the entire expanded concentration range. Some of the parameters that are directly extractable from the data include the average fiber radius (R) and the internal volume fraction of protein in the fibers (Φ_{Int}). Previous studies also suggested that the internal volume fraction of fibrin in a fiber formed in H_2O ranges between 20 and 30% by volume.[33] This method should also be useful in the determination of the internal solids volume fraction (Φ_{Int}) of other biopolymer systems. Furthermore, the internal volume fraction of protein ranged between 10 and 20% by volume, which was substantially smaller than the values reported previously for fibers formed in H_2O solvents. These lower values could be due to differences in the interaction between the fibers and the solvent in D_2O and H_2O or by differences in the accuracy of the methods. Further study is necessary to determine how the monomer concentration affects the internal structure of fibers formed in H_2O based buffers. The presented analysis can be easily extended to X-ray scattering data (SAXS) which is more appropriate to characterize fibrin and other biopolymers in H_2O.

The internal volume fraction (Φ_{Int}) was found to increase over the whole range of concentrations. Two possible causes for the systematic increase in internal protein volume fraction have been considered and illustrated in Fig. 10. It is possible that, at higher concentrations, individual proteins pack closer together within the fiber. This contraction would lead to a slight decrease in fiber radius and an increase in the protein volume fraction. Another theory is that, as the fibrinogen concentration increases, there is more available free protein to correct potential defects such as vacancies in the internal structure of the fibers. This would also result in an increased internal protein fraction. The characterization of internal protein fraction as a function of concentration

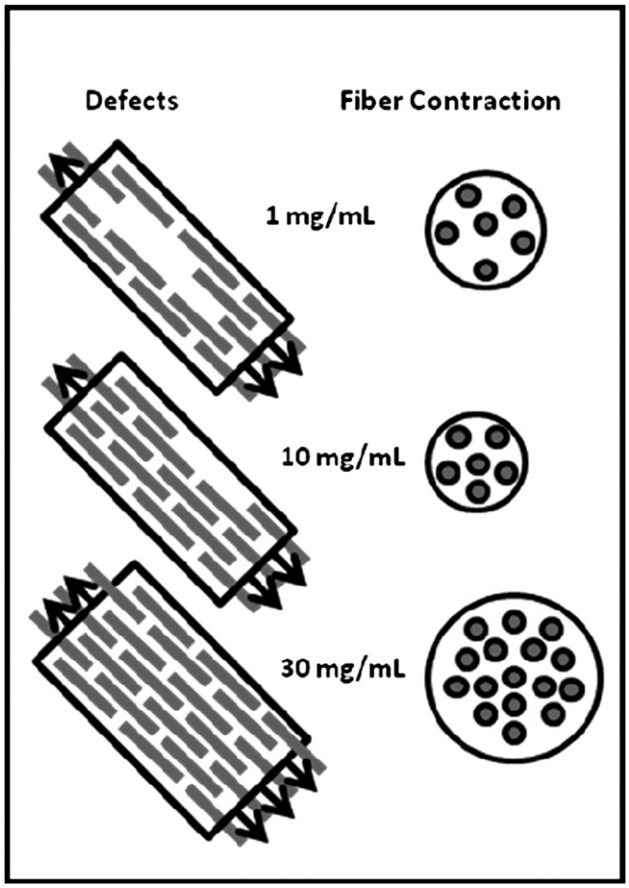

Fig. 10 Illustration of two theories postulated for systematic increase in internal protein fraction. Left: higher fibrinogen to thrombin ratio leads to fewer defects in higher concentration fibers. Right: contraction of proteins within the fiber leading to higher volume fraction with increased concentration.

over such large range of monomer concentration is unique to this work. Also, the ability to characterize structural features of the network and individual fiber is important as it relates to the stability and break up of fibrin clots. Several studies have been published relating variations in the mass–length ratio of fibrin fibers to disease states.[34–36] It has been shown that a lower mass–length ratio, which corresponds to thin fibers, is related to reduced clot permeability and an increased risk of myocardial infarction.[36] Furthermore, the packing density of the protofibril units within the fibers may impact the clot break up even though this has not been explicitly considered in these studies.

Our work shows that there was little variation in the average radius of fibers formed from fibrinogen monomer solutions with concentrations less than 20 mg mL^{-1}. The average number of protofibrils (mass–length ratio) in a fiber cross-section was also found to be nearly constant at 40 protofibrils over this range. This suggests that the increase in internal protein fraction (Fig. 5) was fully offset by the slight decrease in fiber radius (Fig. 6). However, when fibrin concentration was greater than 20 mg mL^{-1} the average radius of the fibers increased sharply to 70 nm and the average number of protofibrils also increased. This change in fibrin structure corresponds to concentrations at which the correlation length, extracted from the fractal model fit, begins to approach the fiber diameter. Initially, as the concentration of the protein increased, the density of the fibrin network also increased but the fiber size remained relatively constant. At larger concentrations, the network is so dense that the fiber structure was altered favoring the formation of thicker fibers. This is corroborated by the increasing fractal dimension and decreasing correlation length obtained from the fractal model. At the highest concentrations examined, 30 and 40 mg mL^{-1} fibrin, the correlation length is approaching the value for the average fiber diameter. This suggests that the increased fiber size may be a result of fiber crowding.

The results presented in this work are specific to fibrin formed in buffer with deuterated water. Deuterated water was used to drive the formation of coarse fibers and to enhance contrast between the solvent and fibrin in the clot. The differences in fibrin conformation caused by using a buffer with D_2O are similar to changes caused by differences in buffer pH or salt concentration. In addition, the enhanced contrast allows both SANS and USANS experiments to be performed on the same samples so that the complete structure of the clots could be seamlessly characterized over length scales ranging from 1 to 15 000 nm. This study is unprecedented in that all relevant length scales are characterized simultaneously and correlated to the rheological behavior of the materials. While it is also possible to use neutron scattering to characterize fibrin formed in an H_2O solvent, the contrast is much smaller and this makes USANS experiments unfeasible. X-Ray scattering techniques such as SAXS and USAXS are more appropriate methods to characterize fibers formed in water.

Conclusions

The results of this study show that SANS and USANS are excellent non-invasive techniques to characterize the structural properties of fibrin clots in aqueous solution at length scales between 1 nm and 15 μm. The analysis of the scattering invariant was an effective method for determining the average internal volume fraction of protein in the fibers. The volume fraction increased systematically with initial monomer concentration. The average radius of the fibers was also determined directly with a Guinier analysis. Finally, the fractal dimension and correlation length were determined by applying a fractal model to the USANS data. The average radius of fibers is found to decrease slightly with increasing concentration until the correlation length approaches the diameter of the fibers. When the gel begins to crowd the fibers begin to grow radially. This change in structural behavior with increased concentration warrants further study as physiological blood clots have high fibrinogen content and also contain platelets and blood cells, which may lead to this crowding condition occurring at even lower concentrations.

Acknowledgements

We wish to acknowledge the helpful comments of Dr Paul Butler and Dr Andrew Jackson regarding this work. This work utilized facilities supported in part by the National Science Foundation under Agreement No. DMR-0454672. We acknowledge the support of the National Institute of Standards and Technology, U.S. Department of Commerce, in providing the neutron

research facilities used in this work. We also acknowledge the financial support of the University of Washington University Initiatives Fund.

References

1 J. P. Collet, H. Shuman, R. E. Ledger, S. T. Lee and J. W. Weisel, *Proc. Natl. Acad. Sci. U. S. A.*, 2005, **102**, 9133–9137.
2 E. A. Ryan, L. F. Mockros, J. W. Weisel and L. Lorand, *Biophys. J.*, 1999, **77**, 2813–2826.
3 F. C. Mackintosh, J. Kas and P. A. Janmey, *Phys. Rev. Lett.*, 1995, **75**, 4425–4428.
4 R. F. Doolittle, *Annu. Rev. Biochem.*, 1984, **53**, 195–229.
5 J. W. Weisel, *Biophys. J.*, 1986, **50**, 1079–1093.
6 M. P. Linnes, B. D. Ratner and C. M. Giachelli, *Biomaterials*, 2007, **28**, 5298–5306.
7 A. Hartmann, P. Boukamp and P. Friedl, *Blood Cells, Mol. Dis.*, 2006, **36**, 191–193.
8 O. V. Gorkun, Y. I. Veklich, L. V. Medved, A. H. Henschen and J. W. Weisel, *Biochemistry*, 1994, **33**, 6986–6997.
9 C. Storm, J. J. Pastore, F. C. MacKintosh, T. C. Lubensky and P. A. Janmey, *Nature*, 2005, **435**, 191–194.
10 P. R. Onck, T. Koeman, T. van Dillen and E. van der Giessen, *Phys. Rev. Lett.*, 2005, **95**, 4.
11 J. W. Weisel, *Biophys. Chem.*, 2004, **112**, 267–276.
12 Z. Yang, I. Mochalkin and R. F. Doolittle, *Proc. Natl. Acad. Sci. U. S. A.*, 2000, **97**, 14156–14161.
13 U. Larsson, *Eur. J. Biochem.*, 1988, **174**, 139–144.
14 M. E. Carr and J. Hermans, *Macromolecules*, 1978, **11**, 46–50.
15 W. A. Voter, C. Lucaveche and H. P. Erickson, *Biopolymers*, 1986, **25**, 2375–2384.
16 J. V. Shah and P. A. Janmey, *Rheol. Acta*, 1997, **36**, 262–268.
17 S. Anand and S. L. Diamond, *Circulation*, 1996, **94**, 763–774.
18 J. J. Pisano, J. S. Finlayson and M. P. Peyton, *Science*, 1968, **160**, 892–893.
19 C. J. Glinka, J. G. Barker, B. Hammouda, S. Krueger, J. J. Moyer and W. J. Orts, *J. Appl. Crystallogr.*, 1998, **31**, 430–445.
20 S. R. Kline, *J. Appl. Crystallogr.*, 2006, **39**, 895–900.
21 J. G. Barker, C. J. Glinka, J. J. Moyer, M. H. Kim, A. R. Drews and M. Agamalian, *J. Appl. Crystallogr.*, 2005, **38**, 1004–1011.
22 J. M. Freyssinet, J. Torbet, G. Hudryclergeon and G. Maret, *Proc. Natl. Acad. Sci. U. S. A.*, 1983, **80**, 1616–1620.
23 M. F. Muller, J. D. Ferry and J. S. Lin, *Biopolymers*, 1989, **28**, 1011–1018.
24 G. Caracciolo, M. De Spirito, A. C. Castellano, D. Pozzi, G. Amiconi, A. De Pascalis, R. Caminiti and G. Arcovito, *Thromb. Haemostasis*, 2003, **89**, 632–636.
25 O. K. O. Glatter, *Small Angle X-ray Scattering*, Academic Press, London, New York, 1982.
26 O. Spalla, *Neutrons, X-rays, and Light: Scattering Applied to Soft Condensed Matter*, Elsevier, Amsterdam, 1st edn, 2002.
27 P. Terech, E. Ostuni and R. G. Weiss, *J. Phys. Chem.*, 1996, **100**, 3759–3766.
28 S. Shulman, *J. Am. Chem. Soc.*, 1953, **75**, 5846–5852.
29 J. Teixeira, *J. Appl. Crystallogr.*, 1988, **21**, 781–785.
30 M. De Spirito, G. Arcòvito, M. Papi, M. Rocco and F. Ferri, *J. Appl. Crystallogr.*, 2003, **36**, 636–641.
31 Q. Wen, A. Basu, J. P. Winer, A. Yodh and P. A. Janmey, *New J. Phys.*, 2007, 9.
32 P. A. Janmey, U. Euteneuer, P. Traub and M. Schliwa, *J. Cell Biol.*, 1991, **113**, 155–160.
33 M. Guthold, W. Liu, B. Stephens, S. T. Lord, R. R. Hantgan, D. A. Erie, R. M. Taylor and R. Superfine, *Biophys. J.*, 2004, **87**, 4226–4236.
34 M. E. Carr, R. M. Dent and S. L. Carr, *J. Lab. Clin. Med.*, 1996, **128**, 83–88.
35 J. P. Collet, Z. Mishal, C. Lesty, M. Mirshahi, J. Peynet, A. Baumelou, A. Bensman, J. Soria and C. Soria, *Thromb. Haemostasis*, 1999, **82**, 1482–1489.
36 K. Fatah, A. Silveira, P. Tornvall, F. Karpe, M. Blomback and A. Hamsten, *Thromb. Haemostasis*, 1996, **76**, 535–540.

